JOURNAL OF GEOPHYSICAL RESEARCH, VOL. 114, A09212, doi:10.1029/2009JA014306, 2009

A mechanism for electrostatic solitary structures in the Earth's magnetosheath

G. S. Lakhina,[1] S. V. Singh,[1] A. P. Kakad,[1] M. L. Goldstein,[2] A. F. Viñas,[2] and J. S. Pickett[3]

Received 28 March 2009; revised 12 June 2009; accepted 8 July 2009; published 24 September 2009.

[1] Electrostatic solitary waves (ESWs) have been observed in the Earth's magnetosheath region by Cluster. A mechanism for the generation of these structures in terms of electron-acoustic solitons and double layers is discussed. The model simulates the magnetosheath plasma by a four-component plasma system consisting of core electrons, two counterstreaming electron beams, and one type of ions. The analysis is based on the fluid equations and the Poisson equation, and employs the Sagdeev pseudopotential techniques to investigate the solitary waves. The electric field amplitudes, the time durations, and the propagation speeds of the solitary structures predicted by the model are in good agreement with the observed electric fields, pulse widths, and speeds of the electrostatic bipolar pulses.

Citation: Lakhina, G. S., S. V. Singh, A. P. Kakad, M. L. Goldstein, A. F. Viñas, and J. S. Pickett (2009), A mechanism for electrostatic solitary structures in the Earth's magnetosheath, *J. Geophys. Res.*, *114*, A09212, doi:10.1029/2009JA014306.

1. Introduction

[2] Electrostatic solitary waves (ESWs) have been observed in several regions of the Earth's magnetosphere, viz., in the plasma sheet boundary layer [*Matsumoto et al.*, 1994], at/in the bow shock [*Bale et al.*, 1998], the magnetosheath [*Pickett et al.*, 2003, 2005], the polar cap boundary layer [*Franz et al.*, 1998; *Tsurutani et al.*, 1998], and on the auroral field lines [*Ergun et al.*, 1998; *Bounds et al.*, 1999; *Pickett et al.*, 2004]. The electrostatic solitary structures are observed in the electric field component parallel to the background magnetic field, and are usually bipolar or tripolar. The amplitudes of ESWs greatly vary from region to region, for example, from less than 100 μV/m in the foreshock region [*Shin et al.*, 2008], 100s of mV/m in the polar region at Polar altitudes [*Cattell et al.*, 1999] and up to 2.5 V/m in the auroral acceleration region [*Ergun et al.*, 1998].

[3] The ESWs are generally associated with electron or/and ion beams. The ESWs associated with the ion beams observed in the auroral zone have usually negative potentials, and they propagate at velocities of the order of ion-acoustic or ion beam speed [*Temerin et al.*, 1982; *Boström et al.*, 1988; *Koskinen et al.*, 1990]. The negative potential ESWs have been interpreted in terms of ion solitary waves or solitons [*Koskinen et al.*, 1990; *Hudson et al.*, 1983; *Reddy and Lakhina*, 1991; *Reddy et al.*, 1992]. In other regions of the Earth's magnetosphere, the ESWs have usually positive potentials, and they travel at velocities comparable to the electron thermal velocity ($\sim$1000s of km s^{-1}). The positive potential ESWs have been commonly interpreted in terms of Bernstein-Greene-Kruskal (BGK) modes or phase-space holes [*Bernstein et al.*, 1957; *Schamel*, 1982; *Muschietti et al.*, 1999; *Jovanovic and Shukla*, 2000; *Chen et al.*, 2005]. Other favorite interpretations for these ESWs are based on the nonlinear evolution of electron two stream instabilities [*Singh and Schunk*, 1984; *Singh et al.*, 1987; *Omura et al.*, 1996; *Kojima et al.*, 1997; *Goldman et al.*, 1999; *Singh et al.*, 2001a; *Singh and Khazanov*, 2003], and electron-acoustic solitary waves [*Pottelette et al.*, 1990, 1999; *Dubouloz et al.*, 1991, 1993; *Berthomier et al.*, 1998, 2000; *Singh et al.*, 2001b; *Singh and Lakhina*, 2001, 2004; *Tagare et al.*, 2004; *Cattaert et al.*, 2005; *Kakad et al.*, 2007; *Ghosh et al.*, 2008; *Lakhina et al.*, 2008a, 2008b]. For a detailed discussion of various models, one can refer to *Lakhina et al.* [2000, 2004].

[4] Recently, *Pickett et al.* [2003, 2005] observed bipolar and tripolar pulses of $\sim$25–100 μs durations in the wave electric field data obtained by the Wideband plasma instrument on the Cluster spacecraft in the dayside magnetosheath region. These pulses represent solitary potential structures and appeared to be electron phase-space holes. *Pickett et al.* [2005] found that within the magnetosheath, solitary waves are likely to be observed at any distance from the shock and that this distance has no dependence on the time durations and amplitudes of the solitary waves. Further, both the time durations and the amplitudes of the solitary waves, show no dependence on either the ion velocity or the angle between the ion velocity and the local magnetic field direction. On the other hand, the solitary waves were generally observed when there are counterstreaming (approximately parallel and antiparallel to the magnetic field) electrons at or below about 100 eV. On the basis of these results, *Pickett et al.*

[1]Upper Atmospheric Studies, Indian Institute of Geomagnetism, Navi Mumbai, India.
[2]Geospace Physics Laboratory, Goddard Space Flight Center, Greenbelt, Maryland, USA.
[3]Department of Physics and Astronomy, University of Iowa, Iowa City, Iowa, USA.

0148-0227/09/2009JA014306$09.00

[2005] concluded that some of the near-Earth magnetosheath solitary waves, perhaps in the form of electron phase-space holes, may be generated locally by a two-stream instability involving counterstreaming electrons that are often observed when solitary waves are present. However, they did not rule out the possibility of solitary wave generation as a result of the lower-hybrid Buneman instability in the presence of an electron beam, through the electron-acoustic mode or through processes involving turbulence.

[5] Recently, *Lakhina et al.* [2008a] studied a three-component plasma system consisting of cold and hot electrons and one species of ions. Solitary wave solutions were found when the Mach numbers exceed some critical values. The critical Mach numbers for the ion-acoustic solitons are found to be smaller than those for electron-acoustic solitons for a given set of plasma parameters. The ion-acoustic solitons had positive potentials for the parameters considered. However, the electron-acoustic solitons could have either positive or negative potentials depending on whether the fractional cold electron density with respect to the ion density was greater or less than a certain critical value. In this paper, we extend the work of *Lakhina et al.* [2008a] to the case of four-component plasma system consisting of core electrons, two counterstreaming electron beams and one species of ions. This model appears capable of simulating the magnetosheath observations of electron and ion distributions during or close to the time of solitary wave observations.

[6] In section 2, we briefly discuss the solitary wave observations in the magnetosheath. Section 3 describes the theoretical model. Section 4 discusses the application to magnetosheath solitary waves. Section 5 gives the summary.

2. Electrostatic Solitary Waves in the Magnetosheath

[7] A sample of electrostatic solitary waves in the magnetosheath observed by two of the four Cluster spacecraft (SC3 and SC4) on 26 March 2002 is shown in Figure 1 which is taken from the work of *Pickett et al.* [2005]. The Cluster spacecraft crossed the bow shock at about 03:19 UT from the solar wind into the magnetosheath at about 15 R_E, 13–14° geomagnetic latitude, and 10:30 Magnetic Local Time (MLT). The top of Figure 1a show the plasma wave spectrum obtained from the Cluster's Wideband (WBD) Plasma Wave Receiver [*Gurnett et al.*, 1997]. This spectrogram has increasing time, in UT, plotted on the horizontal axis and frequency, in kHz, on the vertical axis with color indicating power spectral density, in $V^2m^{-2}Hz^{-1}$. The electron plasma frequency obtained from the Whisper sounder [*Décréau et al.*, 1997] is shown as an overplotted white line in Figures 1a and 1b. It is seen that broadband waves up to and greater than the electron plasma frequency (white line) are observed in the magnetosheath on both spacecraft.

[8] Figure 1b shows a 4-ms line plot of the waveforms beginning at 03:26:22.181 UT. These waveforms were obtained by WBD on SC4 during the 35-min interval seen in the spectrogram (Figure 1a, bottom). The line plot in Figure 1b has increasing time, in seconds from 03:26:22.181 UT, plotted on the horizontal axis and electric field amplitude, in mV/m, plotted on the vertical axis. The total angle of the electric field antenna used by WBD to the local magnetic field using transformed FGM data is plotted as a red line with the scale shown on the right vertical axis. During the time interval in Figure 1b, we see that the antenna was nearly aligned with the magnetic field direction. It is seen that short-duration bipolar pulses are present through out this 4-ms interval. Solitary waves have time durations of a few tens to a few hundreds of μs and peak-to-peak amplitudes of several hundredths to a few tenths of mV/m. Most of the solitary wave pulses have positive electric field first followed by a negative field. However, a few waves have the negative field first, for example, the one labeled as $\sim$80 μs and the very last one in Figure 1b. WBD cannot determine which of these ESW pulses are the positive potential and which are the negative potentials, or if they are the same potential traveling in opposite directions. Seeing opposite initial polarities interspersed in the small period of time implies that these opposite polarities are not solely caused by the spinning antenna orientation with respect to the direction of travel of the ESWs. It is interesting to note that the spectrogram at the time of the waveform in Figure 1b shows only a broadband signal ranging in frequency from the lower cutoff of the filter around 1 kHz, where its greatest intensity is observed, up to about 50 kHz, where a much lower intensity is observed. The broadband signal results from the fact that the pulses observed in the waveforms in Figure 1b contain all frequencies. When one or more of these pulses are transformed to the frequency domain via Fast Fourier Transform, the expected result is a broadband signal as observed. Thus the broadbands seen in Figure 1a throughout the magnetosheath interval ($\sim$03:20–03:50 UT) indicate that solitary waves are most likely present continuously after crossing the bow shock.

[9] Analysis of the SC4 spacecraft PEACE (Plasma Electron And Current Experiment) [*Johnstone et al.*, 1997] electron data from low-energy electron analyzer (LEEA) and high-energy electron analyzer (HEEA) sensors and covering the same time period as Figure 1 indicated the presence of counterstreaming electron beams at energies primarily at or below 100 eV [*Pickett et al.*, 2005]. Further, the ion data from the Cluster Ion Spectrometry (CIS) [*Rème et al.*, 2001] for the same period as 26 March 2002 event (Figure 1b) showed the ion fluxes covering a very broad energy range from about 10 eV up to 10 keV.

[10] Here we have analysed the PEACE electron data in greater details to derive the information about the characteristics of electron distributions, like densities, temperatures, streaming velocities, etc during the period of Figure 1b. We used the method developed by *Viñas and Gurgiolo* [2009]. We found three populations of electrons, viz., core electrons (having approximately solar wind energies) and two counterstreaming electrons beams. The results are summarized in Table 1. For the purpose of modeling, we will consider only one ion species, viz., protons.

3. Theoretical Model

[11] We model the magnetosheath plasma by an infinite, collisionless and magnetized plasma system consisting of four components, namely, core electrons (N_{ce}, T_{ce}, v_{ce}), an electron beam propagating parallel to the magnetic field (N_{pe}, T_{pe}, v_{pe}), and electron beam propagating antiparallel to the magnetic field (N_{ae}, T_{ae}, v_{ae}) and ions (N_i, T_i, v_i), where

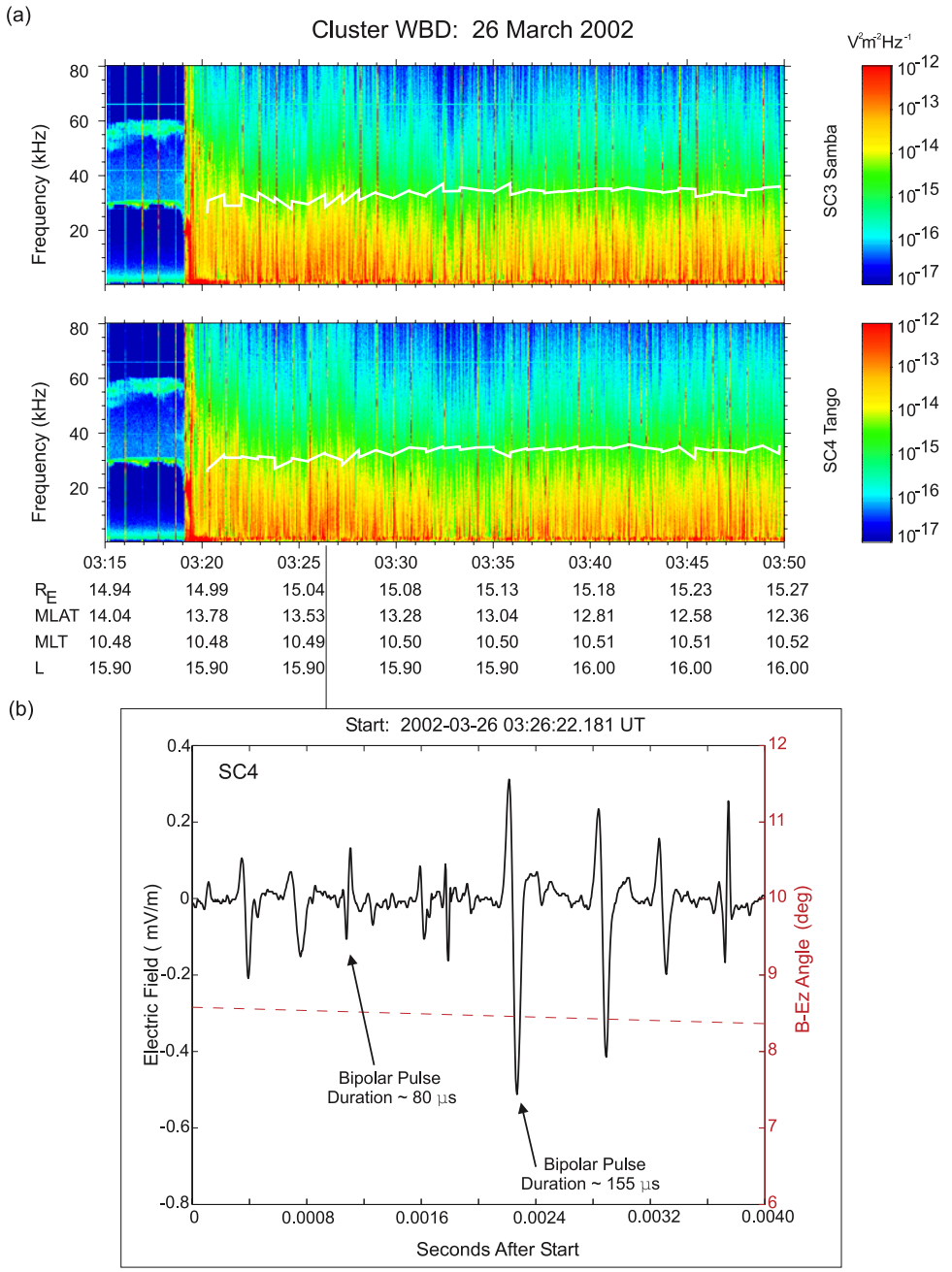

Figure 1. A sample of electrostatic solitary waves in the magnetosheath observed by two of the four Cluster spacecrafts (SC3 and SC4) on 26 March 2002. (a) WBD spectrogram of plasma waves observed by (top) SC3 and (bottom) SC4 as they crossed into the magnetosheath at about 03:19 UT. Broadband waves up to and greater than the electron plasma frequency (white line) are observed in the magnetosheath on both spacecraft. (b) A 4-ms portion of the waveforms from which the spectrograms in Figure 1a were produced. Note the short-duration bipolar pulses seen throughout the 4-ms interval. These bipolar pulses are the primary reason for the broadbands seen in Figure 1a. Taken from the work of *Pickett et al.* [2005].

N_j, T_j, v_j represents the equilibrium values of the density, temperature and beam velocity (along the direction of wave propagation) of the species j, and $j = ce$, pe, ae and i for the core electrons, parallel propagating beam electrons, antiparallel propagating beam electrons, and the ions, respectively. We treat all the species as mobile and consider only the nonlinear electrostatic waves propagating parallel to the magnetic field, in which case their dynamics is governed by the multifluid equations of continuity, momentum, and equation of state of each species, and the Poisson equation [*Lakhina et al.*, 2008a].

$$\frac{\partial n_j}{\partial t} + \frac{\partial (n_j v_j)}{\partial x} = 0 \tag{1}$$

Table 1. Electron Properties During Observations of Magnetosheath Solitary Waves by Cluster on 26 March 2002[a]

Event	Time (h:min:s)	N_{ce} (cm^{-3})	T_{ce} (eV)	v_{ce} (km s^{-1})	N_{pe} (cm^{-3})	T_{pe} (eV)	v_{pe} (km s^{-1})	N_{ae} (cm^{-3})	T_{ae} (eV)	v_{ae} (km s^{-1})
1	03:26:00.72	6.66	45.83	11.013	3.00	20.69	3824.78	2.23	14.19	−4013.12
2	03:26:12.72	6.39	47.98	−49.67	2.74	20.68	3790.22	2.17	14.80	−4236.26
3	03:26:16.74	6.71	48.72	−6.32	2.82	21.98	3997.91	2.33	15.10	−4172.83
4	03:26:24.72	6.40	47.29	41.76	2.88	22.69	3961.88	1.90	12.75	−4043.87
5	03:26:32.70	6.37	51.40	−69.52	2.63	23.76	4064.43	1.98	15.37	−4382.74
6	03:26:40.68	6.21	52.74	21.07	2.52	22.38	3974.68	1.93	15.65	−4204.78
7	03:26:48.72	6.46	53.64	50.04	2.58	24.49	4267.62	1.92	16.12	−4294.07
8	03:26:52.68	6.56	54.04	−42.24	2.41	23.15	4096.48	1.92	16.49	−4528.97

[a]See section 3 for a description of variables.

$$\frac{\partial v_j}{\partial t} + v_j \frac{\partial v_j}{\partial x} + \frac{1}{\mu_j n_j}\frac{\partial P_j}{\partial x} - \frac{Z_j}{\mu_j}\frac{\partial \phi}{\partial x} = 0 \tag{2}$$

$$\frac{\partial P_j}{\partial t} + v_j \frac{\partial P_j}{\partial x} + 3P_j \frac{\partial v_j}{\partial x} = 0 \tag{3}$$

$$\frac{\partial^2 \phi}{\partial x^2} = n_{ce} + n_{pe} + n_{ae} - n_i \tag{4}$$

Here, $\mu_j = m_j/m_i$ (here, m_j and m_i represent the mass of the jth species and the ions, respectively) and $Z_j = +1$ (-1) for electrons (ions), respectively. Further, all densities are normalized with the unperturbed ion density, $N_i = N_{ce} + N_{pe} + N_{ae}$, velocities with the ion thermal velocity $C_i = (T_i/m_i)^{1/2}$, time with the inverse of ion plasma frequency, $\omega_{pi} = (4\pi N_i e^2/m_i)^{1/2}$, the lengths with the ion Debye length, $\lambda_{di} = (T_i/4\pi N_i e^2)^{1/2}$, the electrostatic potential ϕ by T_i/e, and the thermal pressures P_j with $N_i T_i$. Furthermore, we have assumed the same adiabatic index, i.e., $\gamma = 3$, for all the species in the equation of state given by equation (3).

[12] To study the properties of stationary arbitrary amplitude electrostatic solitary waves, we transform the above set of equations to a stationary frame moving with velocity V, the velocity of the solitary wave, i.e., $\xi = (x - Mt)$ where $M = V/C_i$ is the Mach number with respect to the ion thermal velocity. Then, solving for perturbed densities, putting these expressions in the Poisson equation, and assuming appropriate boundary conditions for the localized disturbances along with the conditions that $\phi = 0$, and $d\phi/d\xi = 0$ at $\xi \rightarrow \pm\infty$, we get the following energy integral

$$\frac{1}{2}\left(\frac{\partial \phi}{\partial \xi}\right)^2 + \psi(\phi, M) = 0 \tag{5}$$

where

$$\begin{aligned}
\psi(\phi, M) \;=\; & \mu n_{ce}^0 \left\{ (M - v_{ce})^2 - \frac{(M - v_{ce})}{\sqrt{2}} B_{ce}^{1/2} \right\} \\
& + n_{ce}^0 T_{ce} \left\{ 1 - 2\sqrt{2}(M - v_{ce})^3 B_{ce}^{-3/2} \right\} \\
& + \mu n_{pe}^0 \left\{ (M - v_{pe})^2 - \frac{(M - v_{pe})}{\sqrt{2}} B_{pe}^{1/2} \right\} \\
& + n_{pe}^0 T_{pe} \left\{ 1 - 2\sqrt{2}(M - v_{pe})^3 B_{pe}^{-3/2} \right\} \\
& + \mu n_{ae}^0 \left\{ (M - v_{ae})^2 - \frac{(M - v_{ae})}{\sqrt{2}} B_{ae}^{1/2} \right\} \\
& + n_{ae}^0 T_{ae} \left\{ 1 - 2\sqrt{2}(M - v_{ae})^3 B_{ae}^{-3/2} \right\} \\
& + n_i^0 \left\{ (M - v_i)^2 - \frac{(M - v_i)}{\sqrt{2}} B_i^{1/2} \right\} \\
& + n_i^0 \left\{ 1 - 2\sqrt{2}(M - v_i)^3 B_i^{-3/2} \right\}
\end{aligned} \tag{6}$$

is the pseudopotential, also known as the Sagdeev potential. Here

$$B_{ce} = A_{ce} \pm \sqrt{A_{ce}^2 - \frac{12T_{ce}(M - v_{ce})^2}{\mu}},$$

$$B_{pe} = A_{pe} \pm \sqrt{A_{pe}^2 - \frac{12T_{pe}(M - v_{pe})^2}{\mu}},$$

$$B_{ae} = A_{pe} \pm \sqrt{A_{ae}^2 - \frac{12T_{ae}(M - v_{ae})^2}{\mu}},$$

$$B_i = A_i \pm \sqrt{A_i^2 - 12(M - v_i)^2},$$

$$A_{ce} = (M - v_{ce})^2 + \frac{3T_{ce}}{\mu} + \frac{2\phi}{\mu},$$

$$A_{pe} = (M - v_{pe})^2 + \frac{3T_{pe}}{\mu} + \frac{2\phi}{\mu},$$

$$A_{ae} = (M - v_{ae})^2 + \frac{3T_{ae}}{\mu} + \frac{2\phi}{\mu},$$

$$A_i = (M - v_i)^2 + 3 - 2\phi, \mu = \frac{m_e}{m_i}.$$

[13] In equation (6), $n_j^0 = N_j/N_i$ such that $n_{ce}^0 + n_{pe}^0 + n_{ae}^0 = n_i^0 = 1$, and the temperatures of the species are normalized with the ion temperature. It is interesting to note that equation (5) describes the motion of a pseudo particle of unit mass in a pseudopotential ψ where ϕ and ξ play the role of displacement x from the equilibrium and time, respectively. To solve equation (6), care should be taken in choosing the sign of the second term on the R.H.S. of various B_js as these expressions are respectively related to the densities squared of the jth species. In order that various B_js are real and the associated densities attain their undisturbed values in the limit of $\phi \rightarrow 0$ when $\xi \rightarrow \pm\infty$, we must use the + (plus) sign when the condition $(M - v_j)^2 + \frac{2\phi}{\mu} > \frac{3T_j}{\mu}$ is satisfied, and the − (minus) sign when $(M - v_j)^2 + \frac{2\phi}{\mu} < \frac{3T_j}{\mu}$ holds [*Verheest et al.*, 2008].

4. Soliton and Double Layer Solutions

[14] Equation (5) yields soliton solutions when the Sagdeev potential $\psi(\phi, M)$ satisfies the following conditions: $\psi(\phi, M) = 0$, $d\psi(\phi, M)/d\phi = 0$, $d^2\psi(\phi, M)/d\phi^2 < 0$ at $\phi = 0$; $\psi(\phi, M) = 0$ at $\phi = \phi_0$, and $\psi(\phi, M) < 0$ for $0 < |\phi| < |\phi_0|$. When these conditions are satisfied, the pseudoparticle is reflected in the pseudopotential field and returns to its initial state (zero potential drop) for the solitary wave solution. A different class of nonlinear solutions, namely, double layer solutions, could also exist at an upper limit

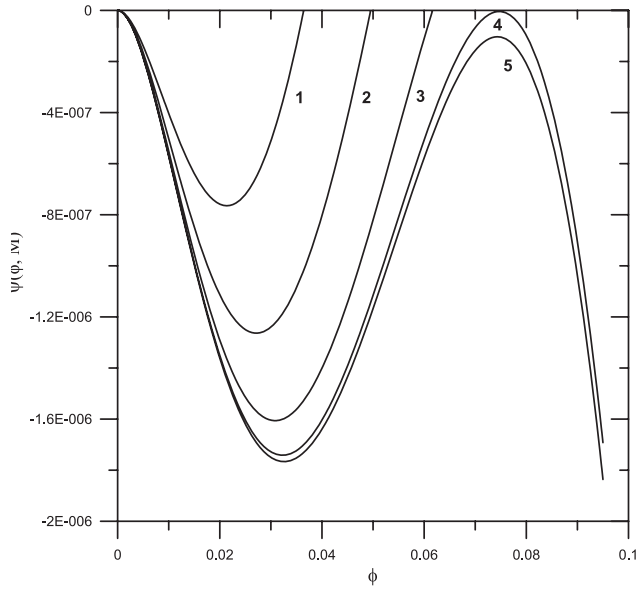

Figure 2. Variation of Sagdeev potential ψ versus the electrostatic potential ϕ of the electron-acoustic solitons for the plasma parameters for event 3 (see Table 1), and for the Mach number M = 65.23, 65.25, 65.26, 65.2634, and 65.264 for curves 1, 2, 3, 4, and 5, respectively.

on the Mach number $M = M_{DL}$ (cf. curve 4 of Figures 2 and 3) provided one more additional condition given below is satisfied.

$$\frac{d\psi(\phi, M)}{d\phi}|_{\phi=\phi_{DL}, M=M_{DL}} = 0 \tag{7}$$

When equation (7) and the above conditions are satisfied, the pseudoparticle is not reflected at $\phi = \phi_{DL}$ because of the vanishing pseudoforce and pseudovelocities. Instead, it goes to another state producing an asymmetrical double layer (DL) with a net potential drop of ϕ_{DL}, where ϕ_{DL} is the amplitude of the double layer.

[15] From equation (6) it is seen that $\psi(\phi, M)$ and its first derivative with respect to ϕ vanish at $\phi = 0$. The condition $d^2\psi(\phi, M)/d\phi^2 < 0$ at $\phi = 0$ is satisfied provided $M > M_0$, where M_0 satisfies the equation

$$f(M_0) \equiv \frac{n_{ce}^0}{\mu\left[(M_0 - v_{ce})^2 - \frac{3T_{ce}}{\mu}\right]} + \frac{n_{pe}^0}{\mu\left[(M_0 - v_{pe})^2 - \frac{3T_{pe}}{\mu}\right]} + \frac{n_{ae}^0}{\mu\left[(M_0 - v_{ae})^2 - \frac{3T_{ae}}{\mu}\right]} + \frac{n_i^0}{\left[(M_0 - v_i)^2 - 3\right]} = 0 \tag{8}$$

Equation (8) yields 6 roots but all the roots will not be physical. We will consider here only the real positive roots for M_0, or the critical Mach numbers. Numerical solution of equation (8), in general yields three critical positive Mach numbers corresponding to an ion-acoustic and two (slow and fast) electron-acoustic beam modes. However, for a given set of plasma parameters, any one, two or all the three modes can satisfy the soliton conditions given above.

[16] We solved equation (8) for the magnetosheath electron parameters given in Table 1. In addition, we neglected the small core electron velocity and considered the proton thermal energy ~100 eV. We find only one positive critical Mach number, M_0, apparently related to electron-acoustic beam mode, which yields soliton and/or double layer solution (as confirmed by subsequent Sagdeev potential analysis). We may point out that without doing a detailed linear analysis, it is not possible to be absolutely sure about the nature of the mode. However, since the critical Mach numbers are large, i.e., $M_0 \sim 60$ or larger, it must involve electron-electron two stream interactions, thus ruling out ion-acoustic mode. Since we have 3 types of electron populations with different temperatures, the existence of electron-acoustic mode is the distinct possibility in such a system [*Singh and Khazanov*, 2003; *Lakhina et al.*, 2008a, 2008b]. However, the possibility of a Langmuir type mode involving counterstreaming electron beams cannot be ruled out.

[17] The Sagdeev potential analysis also gives the upper limit on M (which simply equals M_{DL} when equation (7) is satisfied). For $M > M_{DL}$, no soliton or double layer can exist as at least one B_j no longer remains real leading to an unphysical situation where the species densities become complex. The range of Mach numbers for which electron-acoustic solitons/double layers exists, i.e., $M_0 < M \leq M_{DL}$, are given in Table 2 for all the 8 events of Table 1 (cf., column 2).

[18] We have numerically solved equation (6) for the Sagdeev potential, $\psi(\phi, M)$, as a function of ϕ for various values of Mach numbers above the critical values given in Table 2, column 2. Here, we show the results only for the events 3 and 4 in Figures 2 and 3, respectively. The events 3 and 4 correspond to the time 03:26:16.74 UT and

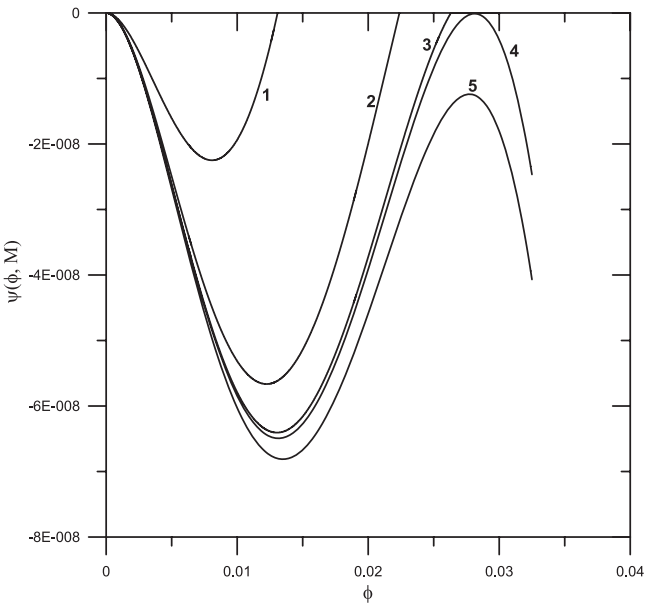

Figure 3. Variation of Sagdeev potential ψ versus the electrostatic potential ϕ of the electron-acoustic solitons for the plasma parameters for event 4, and for the Mach number M = 64.55, 64.56, 64.561, 64.56112, and 64.5615 for curves 1, 2, 3, 4 and 5, respectively.

Table 2. Properties of Electron-Acoustic Solitons[a]

Event	Range of Mach Number, $M_0 < M < M_{max}$	Double Layer	Range of Potential, ϕ	Soliton Width, W	E Range
1	62.56–62.5869	Yes	0.0034–0.0224	116–134	4.33×10^{-5}–3.1×10^{-4}
2	63.05–63.18	Yes	0.0013–0.054	38–80	2.87×10^{-4}–1.43×10^{-3}
3	65.15–65.2633	Yes	0.01–0.073	40–98	2.78×10^{-4}–1.86×10^{-3}
4	64.53–64.5611	Yes	0.0064–0.0262	80–136	9×10^{-5}–3.6×10^{-4}
5	67.05–67.317	Yes	0.0013–0.1	70–80	2.0×10^{-5}–3.0×10^{-3}
6	66.23–66.53575	Yes	0.0027–0.106	50–94	5.5×10^{-5}–3.4×10^{-3}
7	69.13–69.443	Yes	0.003–0.12	65–87	5.2×10^{-5}–3.5×10^{-3}
8	68.09–68.85	No	0.0012–0.1462	28–56	2.4×10^{-5}–7.9×10^{-3}

[a]Here the electrostatic potential ϕ, soliton width W and the electric field E are normalized with T_i/e, ion Debye length λ_{Di}, and $T_i/e\lambda_{Di}$, respectively (cf., section 3).

03:26:24.72 UT, respectively. Therefore the event 3 occurred about 6 s before and the event 4 about 2 s after the ESWs shown in Figure 1b [cf. *Pickett et al.*, 2005].

[19] In Figure 2 it is seen that the electron-acoustic solitons have positive potentials. The maximum electrostatic potential ϕ_0 increases with the increase of the Mach number, M, as seen from the curves 1, 2, 3 and 4 of Figure 2. For curve 5, the soliton solution does not exist. Hence there is an upper value for M, say M_{max}, above which soliton solutions do not exist. Here, $M_{max} = M_{DL}$ as the double layer condition given by equation (7) is satisfied (cf., curve 4). Figure 3 shows the positive potential electron-acoustic solitons for the event 4. The solitons exist for somewhat smaller Mach numbers than for the event 3. Once again we get the double layer solution for M_{DL} close to the M corresponding to curve 4 of Figure 3. The solitary solutions do not exist for M exceeding M_{DL} (cf., curve 5).

[20] In Figures 4 and 5, we have shown the profiles for the potential, ϕ, of the electron-acoustic solitons for different values of Mach numbers M (noted on the curves) for the events 3 and 4. The results for the other events are similar and hence not shown. It is seen that both the amplitude and the width of the electron-acoustic solitons increase with the increase of M. The maximum soliton potentials, ϕ_{max}, are larger and the solitons widths W, defined as full width at half maximum, are smaller for the event 3 (cf., Figure 4) as compared to that of event 4 (cf., Figure 5). The ranges of ϕ_{max} and W for all the 8 events are given in Table 2.

[21] Figures 6 and 7 show the electric field profiles of electron-acoustic solitons (a) and double layers (b) corresponding to the events 3 and 4, respectively. From Figures 6a and 7a, it is clear that electric field profile has a bipolar structure for the electron-acoustic solitons. On the other hand, the electric field profile for the double layers has a monopolar structure as seen from Figures 6b and 7b.

5. Discussion and Conclusions

[22] The model allows the existence of electron-acoustic solitons and double layers for the magnetosheath plasma parameters. The electron-acoustic solitons are found for all the 8 events listed in Table 1. The electron-acoustic double layers, however, are found only for events 1 to 7. The properties of electron-acoustic solitons and double layers in terms of unnormalized quantities, such as their velocities, V, width, W, time duration, $\tau = W/V$, and magnitude of the electric field are given in Table 3. For each event, the electron-acoustic solitons can exist over a range of V, W, τ and E. However, the double layers have only one value of these parameters (the highest value of the range under columns 2 to 5) for each event, except for event 8 where the double layer solution does not exist. For example, the double layer velocity is simply the highest value of V mentioned under column 2.

[23] The time duration and electric field amplitude of the electron-acoustic solitons/double layers predicted by the models are in the range of 90–450 μs and 0.1–35 mV/m, respectively (cf., column 4 and 5 of Table 3). The predicted time duration of the electron-acoustic solitons are in excellent agreement with the observed bipolar solitary pulses having time durations of $\sim$80 μs to above 150 μs as seen from Figure 1b. Further, the lower range of the predicted electric fields, which corresponds to the Mach numbers close to but above the critical Mach numbers, M_0,

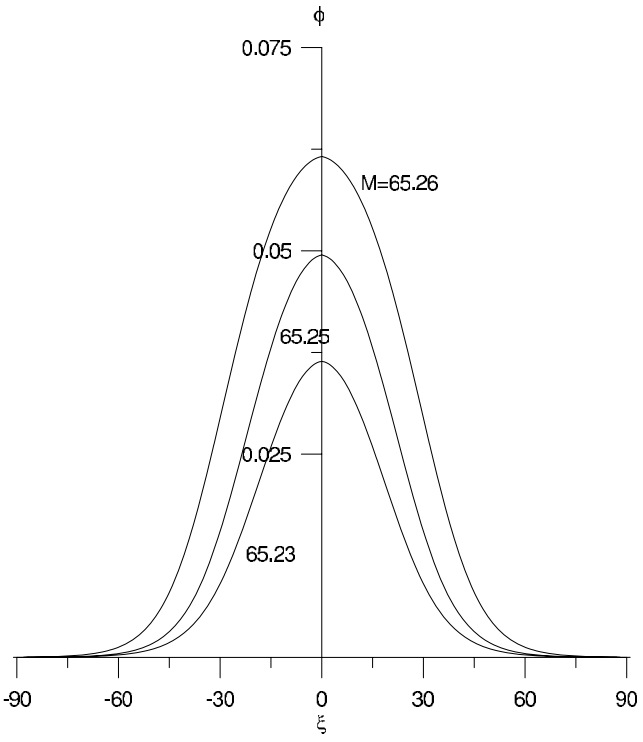

Figure 4. Potential ϕ profiles for the electron-acoustic solitons for the plasma parameters of event 3, and for the Mach number M = 65.23, 65.25, and 65.26.

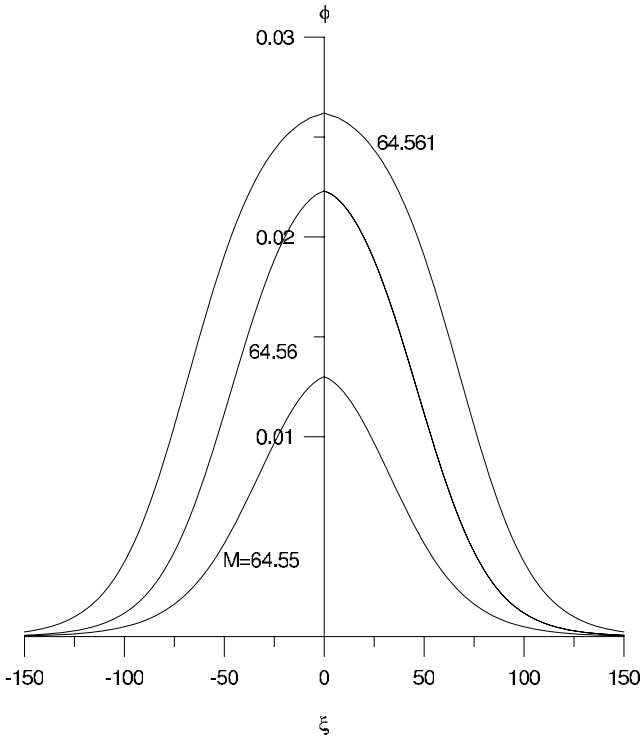

Figure 5. Potential ϕ profiles for the electron-acoustic solitons for the plasma parameters of event 4, and for the Mach number M = 64.55, 64.56, and 64.561.

(column 5 of Table 3) are in very good agreement with the observed electric field of the electrostatic pulses. Furthermore, in Figure 1b, the bipolar pulses (arising presumably from the electron-acoustic solitons) seem to start off with higher time durations, becoming shorter after which the cycle repeats as the time progresses. Nearly similar behavior is seen in the predicted τs from events 1 to 8 (cf. Table 3).

[24] Whereas the bipolar pulses occur frequently in Figure 1b, there are no clear-cut signature of monopolar pulses during the interval of Figure 1b, although there are slight indications of these in the beginning of the interval around 0.0001 s and around 0.0025 s. However, there are clear indications of some of the bipolar pulses being asymmetric with the negative E amplitude larger than the positive E amplitude. It is tempting to suggest that the asymmetry in the amplitude of the bipolar pulses may arise from the superposition of an electron-acoustic soliton (symmetric bipolar pulse) and a double layer (negative amplitude monopolar pulse) propagating at nearly the same speed. The model cannot produce tripolar pulses directly. A particular superposition of two electron-acoustic solitons with a double layer in between may lead to the formation of a tripolar pulse. Such tripolar pulses will always have a large negative value in the center with two small positive shoulders.

[25] We would like to point out that the model developed here does not take into account the effect of the magnetic field on the solitary waves. This is strictly justified for the parallel propagating electrostatic solitary structures. For the obliquely propagating ESWs, one needs to extend the analysis to take into account the ambient magnetic field in the magnetosheath region. This is left for the future investigations of ESWs.

[26] We would like to mention that the electron magnetization plays an important role on the structure as well as stability of the ESWs. From the analysis of the electric field data from the Polar Plasma Wave Instrument, *Franz et al.* [2000] showed that ESWs are roughly spherical for $R = f_{ce}/f_{pe} > 1$, and become more oblate (with perpendicular scale larger than the parallel scale) as R decreases to less that 1. Here, f_{ce} and f_{pe} are the electron cyclotron frequency and the electron plasma frequency, respectively. *Singh et al.* [2001a] carried out 3D particle simulation of electron holes (e-holes) and found that e-holes are essentially planar and highly transitory for $R < 1$ while for $R \geq 2$ they are long lasting and

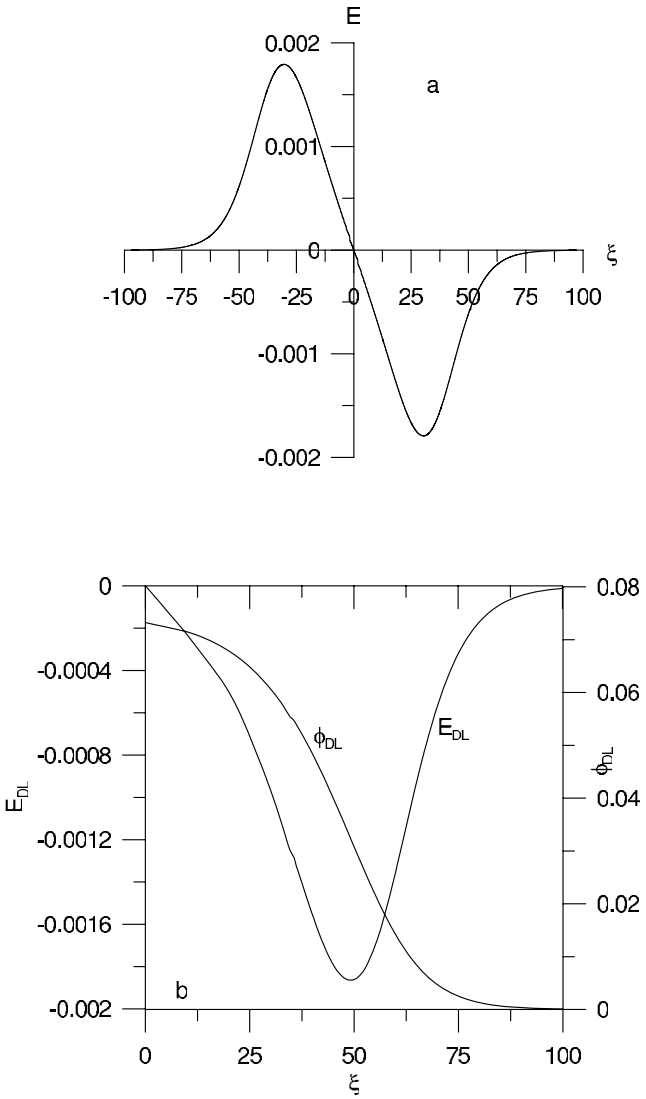

Figure 6. (a) Electric field E profile for the electron-acoustic solitons for the plasma parameters of event 3 and for M = 65.26. The E profile has a bipolar structure. (b) Potential ϕ and electric field E profiles for the electron-acoustic double layer for the plasma parameters of event 3, and for M = 65.2634. The E profile has a monopolar structure.

can have a variety of structures from spherical to planar. For the case of magnetosheath ESWs, during the interval of interest, the electron plasma frequency was $f_{pe} \approx (26-37)$ kHz and electron cyclotron frequency was $f_{ce} \approx (980-1260)$ Hz [*Pickett et al.*, 2005], thus giving $R = (0.025-0.05)$. Since $R \ll 1$, the long-lasting electron phase-space holes are most unlikely to exist in the magnetosheath [*Singh et al.*, 2001a].

[27] To summarize, we have developed a model for the nonlinear ion- and electron-acoustic waves in a four-component plasma system consisting of core electrons, two counterstreaming electron beams and one type of ions.

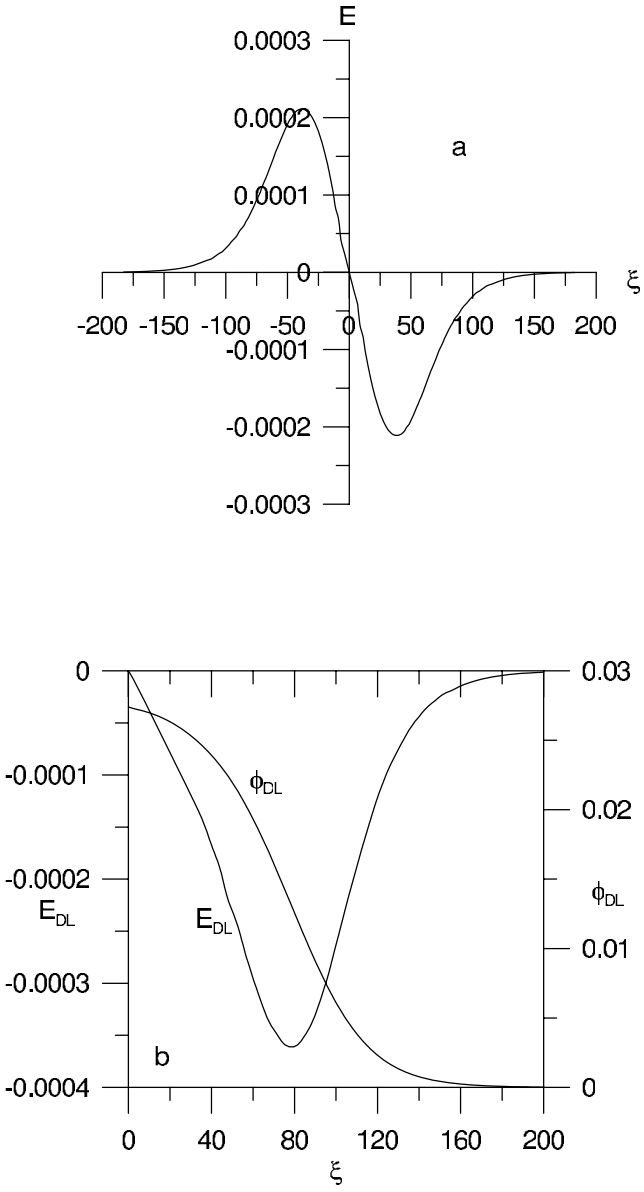

Figure 7. (a) Electric field E profile for the electron-acoustic solitons for the plasma parameters of event 4, and for $M = 64.55$. The E profile has a bipolar structure. (b) Potential ϕ and electric field E profiles for the electron-acoustic double layer for the plasma parameters of event 4, and for $M = 64.561115$. The E profile has a monopolar structure.

Table 3. Properties of Electron-Acoustic Solitons and Double Layers[a]

Event	Range of Allowed Soliton Velocity, V (km s^{-1})	Soliton Width, W (km)	Pulse Duration, τ (μs)	Electric Field, E (mV/m)
1	6125–6127	2.5–2.9	408–473	0.2–1.44
2	6174–6185	0.82–1.72	133–278	1.29–6.5
3	6378–6389	0.862–2.11	135–330	1.28–8.62
4	6319–6321	1.725–2.93	272–463	0.4–1.62
5	6565–6590	1.51–1.72	230–261	0.1–13.2
6	6486–6513	1.08–2.03	166–319	0.24–14.9
7	6770–6800	1.40– 1.88	206–276	0.22–15.59
8	6667–6740	0.6–1.21	90–179	0.1–35

[a]The highest value of the range under columns 2 to 5 is for the double layer for each event, except for event 8 where the double layer solution does not exist.

This model can simulate the magnetosheath observations of electron and ion distributions during or close to the time of solitary wave observations by Cluster spacecraft on 26 March 2002. We analyze the PEACE Electron data for the interval 03:26:00 to 03:26:53 when the ESWs were observed in the magnetosheath (see Table 1). We consider the ions to be protons with energy of ~100 eV; an estimate based on CIS data [*Pickett et al.*, 2005]. When these parameters are used as input, the model predicts the existence of positive potential electron-acoustic solitons and double layers. It is proposed that the bipolar electrostatic solitary structures observed in the Earth's magnetosheath region by Cluster are caused by electron-acoustic solitons and double layers. The predicted electric field amplitudes, pulse widths and propagation speeds of the solitary structures are in good agreement with the observations of ESWs.

[28] **Acknowledgments.** G.S.L. thanks the Indian National Science Academy, New Delhi, for the support under the Senior Scientist scheme. J.S.P. acknowledges support from NASA Goddard Space Flight Center under grant NNX07AI24G.

[29] Zuyin Pu thanks Frank Verheest and another reviewer for their assistance in evaluating this paper.

References

Bale, S. D., P. J. Kellogg, D. E. Larsen, R. P. Lin, K. Goetz, and R. P. Lepping (1998), Bipolar electrostatic structures in the shock transition region: Evidence of electron phase space holes, *Geophys. Res. Lett.*, *25*, 2929–2932.

Bernstein, I. B., J. M. Greene, and M. D. Kruskal (1957), Exact nonlinear plasma oscillations, *Phys. Rev.*, *108*, 546–550.

Berthomier, M., R. Pottelette, and M. Malingre (1998), Solitary waves and weak double layers in a two-electron temperature auroral plasma, *J. Geophys. Res.*, *103*, 4261–4270.

Berthomier, M., R. Pottelette, M. Malingre, and Y. Khotyaintsev (2000), Electron acoustic solitons in an electron-beam plasma system, *Phys. Plasmas*, *7*, 2987–2994.

Boström, R., G. Gustafsson, B. Hollback, G. Holmgren, H. Koskinen, and P. Kintner (1988), Characteristics of solitary waves and double layers in the magnetospheric plasma, *Phys. Rev. Lett.*, *61*, 82–85.

Bounds, S. R., R. F. Pfaff, S. F. Knowlton, F. S. Mozer, M. A. Temerin, and C. A. Kletzing (1999), Solitary potential structures associated with ion and electron beams near 1 R_E altitude, *J. Geophys. Res.*, *104*, 28,709–28,717.

Cattaert, T., F. Verheest, and M. A. Hellberg (2005), Potential hill electron-acoustic solitons and double layers in plasmas with two electron species, *Phys. Plasmas*, *12*, 042901, doi:10.1063/1.1868733.

Cattell, C. A., J. Dombeck, J. R. Wygant, M. K. Hudson, F. S. Mozer, M. A. Temerin, W. K. Peterson, C. A. Kletzing, C. T. Russell, and R. F. Pfaff (1999), Comparisons of Polar satellite observations of solitary wave velocities in the plasma sheet boundary and the high altitude cusp to those in the auroral zone, *Geophys. Res. Lett.*, *26*, 425–428.

Chen, L. J., J. S. Pickett, P. Kintner, J. Franz, and D. A. Gurnett (2005), On the width-amplitude inequality of electron phase space holes, *J. Geophys. Res.*, *110*, A09211, doi:10.1029/2005JA011087.

Décréau, P. M. E., D. Fergeau, V. Krasnoselskikh, M. Lévêque, Ph. Martin, O. Randriamboarison, F. X. Sené, J. G. Trotignon, P. Canu, and P. B. Mgensen (1997), WHISPER, A resonance sounder and wave analyser: Performances and perspectives for the cluster mission, *Space Sci. Rev.*, *79*, 157–193.

Dubouloz, N., R. Pottelette, M. Malingre, and R. A. Treumann (1991), Generation of broadband electrostatic noise by electron acoustic solitons, *Geophys. Res. Lett.*, *18*, 155–158.

Dubouloz, N., R. A. Treumann, R. Pottelette, and M. Malingre (1993), Turbulence generated by a gas of electron acoustic solitons, *J. Geophys. Res.*, *98*, 17,415–17,422.

Ergun, R. E., et al. (1998), FAST satellite observations of large-amplitude solitary structures, *Geophys. Res. Lett.*, *25*, 2041–2044.

Franz, J. R., P. M. Kintner, and J. S. Pickett (1998), POLAR observations of coherent electric field structures, *Geophys. Res. Lett.*, *25*, 1277–1280.

Franz, J. R., P. M. Kintner, C. E. Seyler, J. S. Pickett, and J. D. Scudder (2000), On the perpendicular scale of electron phase-space holes, *Geophys. Res. Lett.*, *27*, 169–172.

Ghosh, S. S., J. S. Pickett, G. S. Lakhina, J. D. Winningham, B. Lavraud, and P. M. E. Décréau (2008), Parametric analysis of positive amplitude electron acoustic solitary waves in a magnetized plasma and its application to boundary layers, *J. Geophys. Res.*, *113*, A06218, doi:10.1029/2007JA012768.

Goldman, M. V., M. M. Oppenheim, and D. L. Newman (1999), Nonlinear Two-Stream Instabilities as an explanation for the auroral bipolar wave structures, *Geophys. Res. Lett.*, *26*, 1821–1824.

Gurnett, D. A., R. L. Huff, and D. L. Kirchner (1997), The Wide-Band plasma wave investigation, *Space Sci. Rev.*, *79*, 195–208.

Hudson, M. K., W. Lotko, I. Roth, and E. Witt (1983), Solitary waves and double layers on auroral field lines, *J. Geophys. Res.*, *88*, 916–926.

Johnstone, A. D., et al. (1997), PEACE: A plasma and electron and current experiment, *Space Sci. Rev.*, *79*, 351–398.

Jovanovic, D., and P. K. Shukla (2000), Nonlinear model for coherent electric field structures in the magnetosphere, *Phys. Rev. Lett.*, *84*, 4373–4376.

Kakad, A. P., S. V. Singh, R. V. Reddy, G. S. Lakhina, S. G. Tagare, and F. Verheest (2007), Generation mechanism for electron acoustic solitary waves, *Phys. Plasmas*, *14*, 052305, doi:10.1063/1.2732176.

Kojima, H., H. Matsumoto, S. Chikuba, S. Horiyama, M. Ashour-Abdalla, and R. R. Anderson (1997), Geotail waveform observations of broadband/narrowband electrostatic noise in the distant tail, *J. Geophys. Res.*, *102*, 14,439–14,455.

Koskinen, H. E. J., R. Lundin, and B. Holback (1990), On the plasma environment of solitary waves and weak double layers, *J. Geophys. Res.*, *95*, 5921–5929.

Lakhina, G. S., B. T. Tsurutani, H. Kojima, and H. Matsumoto (2000), "Broadband" plasma waves in the boundary layers, *J. Geophys. Res.*, *105*, 27,791–27,831.

Lakhina, G. S., B. T. Tsurutani, and J. S. Pickett (2004), Association of Alfven waves and proton cyclotron waves with electrostatic bipolar pulses: Magnetic hole events observed by Polar, *Nonlin. Process. Geophys.*, *11*, 11,205–11,213.

Lakhina, G. S., A. P. Kakad, S. V. Singh, and F. Verheest (2008a), Ion-and electron-acoustic solitons in two-electron temperature space plasmas, *Phys. Plasmas*, *15*, 062903, doi:10.1063/1.2930469.

Lakhina, G. S., S. V. Singh, A. P. Kakad, F. Verheest, and R. Bharuthram (2008b), Study of nonlinear ion- and electron-acoustic waves in multicomponent space plasmas, *Nonlin. Process. Geophys.*, *15*, 903–913.

Matsumoto, H., H. Kojima, T. Miyatake, Y. Omura, Y. M. Okada, I. Nagano, and M. Tsutui (1994), Electrostatic solitary waves (ESW) in the magnetotail: BEN wave forms observed by GEOTAIL, *Geophys. Res. Lett.*, *21*, 2915–2918.

Muschietti, L., R. E. Ergun, I. Roth, and C. W. Carlson (1999), Phase-Space electron holes along magnetic field lines, *Geophys. Res. Lett.*, *26*, 1093–1096.

Omura, Y., H. Matsumoto, T. Miyake, and H. Kojima (1996), Electron beam instabilities as generation mechanism of electrostatic solitary waves in the magnetotail, *J. Geophys. Res.*, *101*, 2685–2697.

Pickett, J. S., J. D. Menietti, D. A. Gurnett, B. T. Tsurutani, P. Kintner, E. Klatt, and A. Balogh (2003), Solitary potential structures observed in the magnetosheath by the Cluster spacecraft, *Nonlin. Process. Geophys.*, *10*, 3–11.

Pickett, J. S., et al. (2004), Solitary waves observed in the auroral zone: The Cluster multi-spacecraft perspective, *Nonlin. Process. Geophys.*, *11*, 183–196.

Pickett, J. S., et al. (2005), On the generation of solitary waves observed by Cluster in the near-Earth magnetosheath, *Nonlin. Process. Geophys.*, *12*, 181–193.

Pottelette, R., M. Malingre, N. Dubouloz, B. Aparicio, R. Lundin, G. Holmgren, and G. Marklund (1990), High frequency waves in the Cusp/cleft regions, *J. Geophys. Res.*, *95*, 5957–5971.

Pottelette, R., R. E. Ergun, R. A. Treumann, M. Berthomier, C. W. Carlson, J. P. McFadden, and I. Roth (1999), Modulated electron-acoustic waves in auroral density cavities: FAST observations, *Geophys. Res. Lett.*, *26*, 2629–2632.

Reddy, R. V., and G. S. Lakhina (1991), Ion-acoustic double layers and solitons in auroral plasma, *Planet. Space Sci.*, *39*, 1343–1350.

Reddy, R. V., G. S. Lakhina, and F. Verheest (1992), Ion-acoustic double layers and solitons in multispecies auroral beam plasmas, *Planet. Space Sci.*, *40*, 1055–1062.

Rème, H., C. Aoustin, J. M. Bosqued, I. Dandouras, and B. Lavraud (2001), First multispacecraft ion measurements in and near the Earth's magnetosphere with the identical Cluster ion spectrometry (CIS) experiment, *Ann. Geophys.*, *19*, 1303–1354.

Schamel, H. (1982), Kinetic theory of phase space vortices and double layers, *Phys. Scr. T*, *2/1*, 228–237.

Shin, K., H. Kojima, H. Matsumoto, and T. Mukai (2008), Characteristics of electrostatic solitary waves in the Earth's foreshock region: Geotail observations, *J. Geophys. Res.*, *113*, A03101, doi:10.1029/2007JA012344.

Singh, N., and G. Khazanov (2003), Double layers in expanding plasmas and their relevance to the auroral plasma processes, *J. Geophys. Res.*, *108*(A4), 8007, doi:10.1029/2002JA009436.

Singh, S. V., and G. S. Lakhina (2001), Generation of electron-acoustic waves in the magnetosphere, *Planet. Space Sci.*, *49*, 107–114.

Singh, S. V., and G. S. Lakhina (2004), Electron acoustic solitary waves with non-thermal distribution of electrons., *Nonlin. Process. Geophys.*, *11*, 275–279.

Singh, N., and R. W. Schunk (1984), Plasma response to the injection of an electron beam, *Plasma Phys. Control. Fusion*, *26*, 859–890, doi:10.1088/0741-3335/26/7/003.

Singh, N., H. Thiemann, and R. W. Schunk (1987), Simulations of auroral plasma processes: Electric fields, waves and particles, *Planet. Space Sci.*, *35*, 353–395.

Singh, N., S. M. Loo, and E. Wells (2001a), Electron hole structure and its stability depending on plasma magnetization, *J. Geophys. Res.*, *106*, 21,183–21,198.

Singh, S. V., R. V. Reddy, and G. S. Lakhina (2001b), Broadband electrostatic noise due to nonlinear electron acoustic waves, *Adv. Space Res.*, *28*(11), 1643–1648.

Tagare, S. G., S. V. Singh, R. V. Reddy, and G. S. Lakhina (2004), Electron acoustic solitons in the Earth's magnetotail, *Nonlin. Process. Geophys.*, *11*, 215–218.

Temerin, M., K. Cerny, W. Lotko, and F. S. Mozer (1982), Observations of double layers and solitary waves in the auroral plasma, *Phys. Rev. Lett.*, *48*, 1175–1179.

Tsurutani, B. T., J. K. Arballo, G. S. Lakhina, C. M. Ho, B. Buti, J. S. Pickett, and D. A. Gurnett (1998), Plasma waves in the dayside polar cap boundary layer: Bipolar and monopolar electric pulses and whistler mode waves, *Geophys. Res. Lett.*, *25*, 4117–4120.

Verheest, F., M. A. Hellberg, and I. Kourakis (2008), Acoustic solitary waves in dusty and/or multi-ion plasmas with cold, adiabatic, and hot constituents, *Phys. Plasmas*, *15*, 112309, doi:10.1063/1.3026716.

Viñas, A. F., and C. Gurgiolo (2009), Spherical harmonic analysis of particle velocity distribution function: Comparison of moments and anisotropies using Cluster data, *J. Geophys. Res.*, *114*, A01105, doi:10.1029/2008JA013633.

M. L. Goldstein and A. F. Viñas, Geospace Physics Laboratory, Code 673, Goddard Space Flight Center, Greenbelt, MD 20771, USA.

A. P. Kakad, G. S. Lakhina, and S. V. Singh, Upper Atmospheric Studies, Indian Institute of Geomagnetism, Plot No. 5, Sector-18, New Panvel (W), Navi Mumbai 410 218, India. (lakhina@iigs.iigm.res.in)

J. S. Pickett, Department of Physics and Astronomy, University of Iowa, Iowa City, IA 52242, USA.